Journal of
Manufacturing and Materials Processing

MDPI

Article

On Forming Characteristics of Hems by Means of Incremental Sheet Forming

Dennis Steinfels * and David Bailly

Institute of Metal Forming, Rheinisch-Westfälische Technische Hochschule Aachen University, Intzestr. 10, 52072 Aachen, Germany; david.bailly@ibf.rwth-aachen.de
* Correspondence: dennis.steinfels@ibf.rwth-aachen.de

Abstract: Given the need for versatile joining processes, form-fit joining is gaining increasing importance. Although it has known limitations and complexity, roller hemming remains widely used due to its flexibility. Here, the novel Incremental Sheet Forming (ISF) hemming technique has the potential to expand the range of applications and process limits. It has already proven effective in preliminary works for joining comparatively small radii without wrinkles and cracks. However, a deeper understanding of the dominant material flow and deformation mechanism during forming is required to fully exploit its potential. This study aims to conduct a detailed examination of this technology through experimental and numerical investigations. Strain measurements on convex and concave hems provide insights into the material flow. A comparison of the forming mechanism for both processes is made using straight hems. The results show that ISF hemming has a favorable material flow for compensating cracks and wrinkles in curved hems. Additionally, it induces strains across the entire hem area, reaching higher values than those achieved with roller hemming. One reason for this is the forming mechanism, which combines tension, compression and shear, whereas roller hemming primarily involves bending and compression of the hemming radius.

Keywords: incremental sheet forming; hemming; joining; forming technology; structural joining; roller hemming; material flow; thinning

Citation: Steinfels, D.; Bailly, D. On Forming Characteristics of Hems by Means of Incremental Sheet Forming. *J. Manuf. Mater. Process.* **2024**, *8*, 266. https://doi.org/10.3390/jmmp8060266

Received: 4 November 2024
Revised: 22 November 2024
Accepted: 23 November 2024
Published: 26 November 2024

1. Introduction

Manufacturing processes for flexible joining are becoming increasingly important against the backdrop of growing product diversity and greater individualization customer products. Customer demands for sophisticated, complex shapes and an ever-increasing mix of materials in consumer products are creating the need for versatile manufacturing processes. One such example is the automotive sector. Here, firmly bonded joining processes such as welding often cannot be used due to incompatible materials. Therefore, form-fit processes such as hemming are used in these areas. At the same time, the variety of shapes and product designs with sharp edges and tight radii is increasing. This in turn restricts the use of conventional hemming processes with presses. This is where the present work follows on from. In addition to the established roller hemming, a new joining process for flexible form-fit joining, ISF hemming, is investigated.

1.1. Hemming and Roller Hemming

Joining by forming, also known as mechanical joining, refers to processes that achieve permanent connections between two or more workpieces by forming one of the joining partners. This typically requires either overlapping areas of the workpieces or additional fasteners such as rivets [1]. Joining by forming can be found in large parts of the automotive and aerospace industries due to its many advantages. These include the ability to join a wide range of different materials and material thicknesses. In addition, there is no thermal influence as with welding, which is why there is no weakening and high residual stresses

in the joined parts. Finally, they have good environmental behavior, as there is hardly any emission or pollution [1].

Hemming and roller hemming also belong to this category. These involve joining an inner structural sheet to an outer panel by folding over an upright flange to produce visually demanding joint edges. Typical examples can be found in car body manufacturing such as hoods, tailgates, and doors, as seen in Figure 1. Hemming and roller hemming are based on the same principle: In several steps, a flange that is initially upright is bent and formed onto an inner sheet as indicated in Figure 2. Typical angles per process stage can vary between 30 and 45 degrees.

Figure 1. Example components with hemmed outer edges.

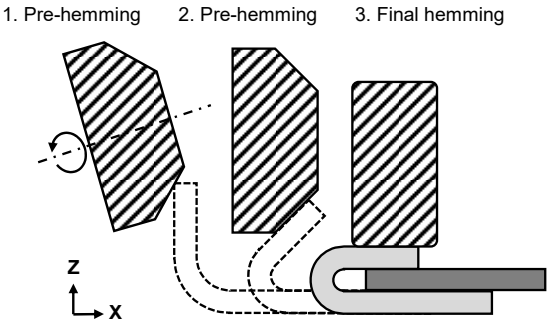

Figure 2. Typical hemming process steps using the example of roller hemming [2].

In addition to joining parts, hemming in general increases the stiffness of the part, eliminates acute edges, and improves appearance [3]. Conventional hemming, also known as table-top hemming, relies on rigid tools in a press, whereas roller hemming utilizes a universal roller, typically guided by a robot along the hemming line. This makes roller hemming much more flexible, as no dedicated tools are required. The advantages of this process include rapid adaptation to new product geometries and low investment costs. The disadvantages in comparison to table-top hemming are the longer process times and the low system stiffness. Within the robot's working space, the effective levers are constantly changing and thus influence the forming force generated by the robot arm [4,5]. However, geometric defects such as wrinkles and cracks are often observed during pre-hemming for both hemming processes [6–8]. The reasons for this are non-uniform tangential compressive stresses and increased compressive stresses when hemming convex edges (cf. Figure 3) [9,10]. In roller hemming, the tendency for wrinkling is higher for smaller roller diameters and greater pre-hemming bending angles.

As table-top hemming is derived from a pure bending process, the observed stresses and strains are localized in the bending radius [11,12]. This includes tensile stresses in the outer fiber of the bending radius and compressive stresses in the inner fiber. In roller hemming, the stress state has an additional tangential component in the rolling direction. The flange is locally elongated in the rolling direction and causes tangential compressive stresses. This also leads to a tendency to wrinkling or surface waves in pre- and final

hemming [13]. Therefore, table-top hemming and roller hemming of sharp contours and small radii still represents a challenge and often requires a so-called flange relief. This is a local reduction in flange length by tailoring the blank as indicated in Figure 4, which allows for the flange to lay flat after the final hemming step [3].

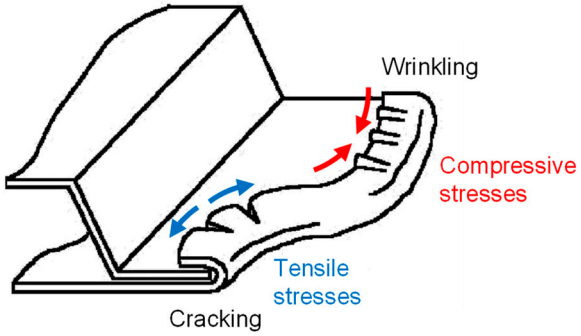

Figure 3. Typical defects for hemming of concave and convex contours [9].

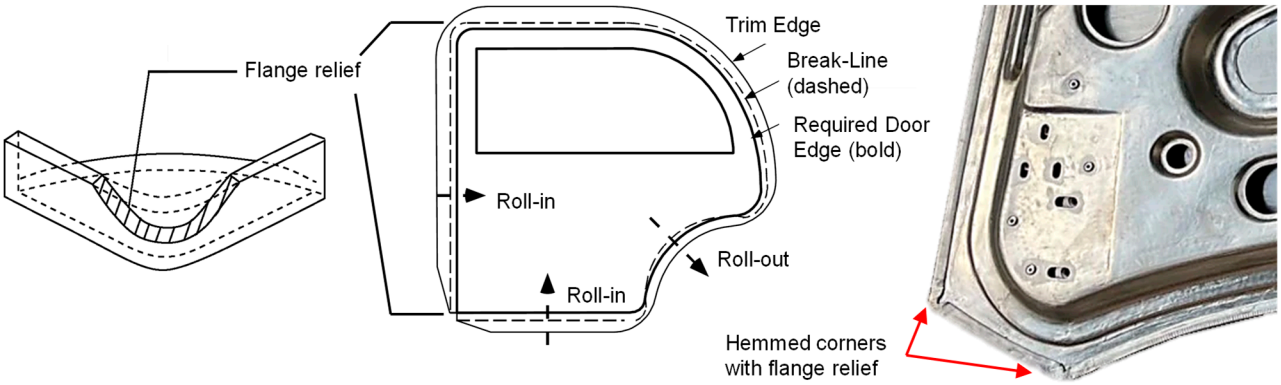

Figure 4. Examples of flange reliefs in sharp corners of hemming products [3,9].

1.2. Hemming by Incremental Sheet Forming

Incremental sheet metal forming (ISF) is an equally flexible process compared to roller hemming. It uses a universal, usually hemispherical tool to incrementally form a target geometry in many passes. It is characterized by high formability and flexibility due to the fast implementation from CAD design to finished components with low requirements for application-specific tools. In past works, ISF has been used for a variety of applications: automotive [14], medical sector [15], architecture [16], hole flanging [17], forming of composite materials [18], and many more. The increased formability is due to localized and successive forming. Since only a local area is formed while the surrounding areas are unclamped, the material can flow and distribute from thickness direction more easily. Here, higher strains are reached before failure, usually allowing for the process limits of conventional methods to be exceeded.

The recent concept of leveraging the benefits of ISF for a new joining method was initially investigated on hole flanges [19]. Similar to hemming, a subsequent joining operation by means of ISF is performed, after the incremental forming of hole flanges. Blanks with different initial diameters (d_0) were widened using a 20 mm ISF tool to flanges with an inner diameter (d_1) of 100 mm, resulting in different flange lengths between 11 and 22 mm. In the final step, these flanges were formed to partial as well as complete form-fit hems, as shown in Figure 5. All joints could be realized without failures like cracks and wrinkles. The resulting geometric deviations were attributed to springback. Overall, the study on joining of closed concave geometries by ISF proved a general feasibility of the process. However, no further investigations on the deformation mechanism or material flow during hemming were carried out [19].

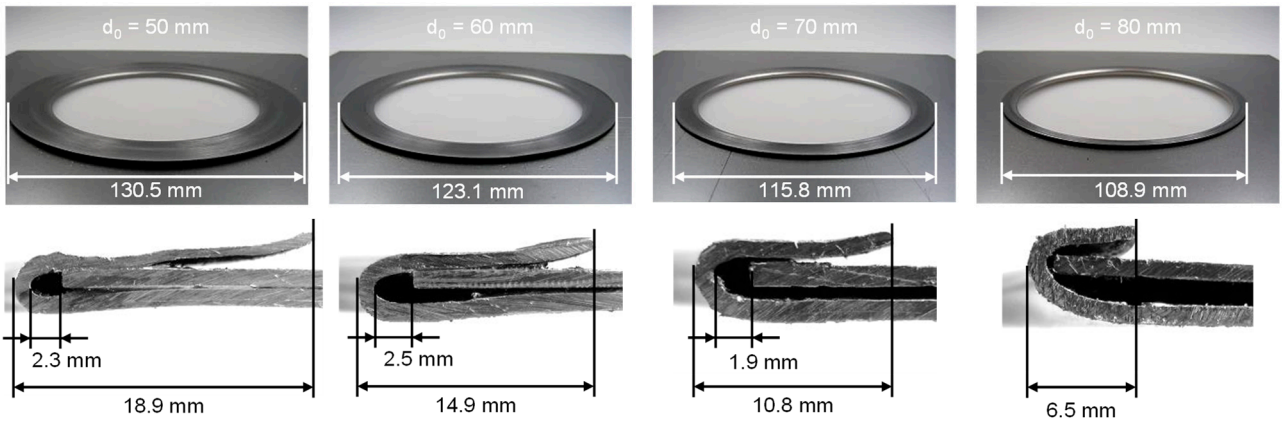

Figure 5. Joint components and their respective cross-sections formed by ISF with different hole diameters [19].

In the previous study, ISF hemming of closed convex edges was investigated in addition to concave edges for edge radii of 200 mm and 50 mm and flange lengths between 5 mm and 20 mm [20]. The study focused on findings related to the material flow induced by ISF during the forming. A hypothesis was set up, positing that increased material flow in radial direction would increase the formability of convex hems by preventing wrinkles. On the other hand, increased material flow in the circumferential direction should help to compensate for the enlarged flange surface in concave hems. An improved material flow was confirmed by measuring the sheet thickness distribution and elongation of the flanges. An increase in sheet thickness for the shrink hems has also been verified. Conclusions about the current state of stress and strain remained to be drawn. This work aims to gain a broader understanding of the present stresses and strains in ISF hemming and to classify it in relation to roller hemming. The procedure for achieving this is explained in the following chapter.

The state of the art points out that further investigations on ISF hemming are needed to fully understand the process and to identify more of its potential. In comparison to roller hemming, a different stress and strain distribution in the hem can be expected for ISF hemming. On one hand, there is a difference in contact area during hemming: roller hemming involves a line contact, while ISF hemming takes the form of a point-shaped contact, as indicated by Figure 6. On the other hand, the processes differ in tool motion. As depicted in Figure 7, during roller hemming, the roller moves over the flange in unidirectional motion with the tool rotating freely due to the friction with the flange. Contrary to this, in ISF hemming, the tool moves in a parallel direction to the hemming edge and adds a perpendicular movement for the subsequent forming path. Therefore, the whole flange is formed over by the end of the process.

The underlying deformation mechanism also differs in both processes. In roller hemming, the deformation is mainly introduced by bending, whereas ISF has an additional shear component perpendicular to the direction of travel. This was shown not only for closed geometries such as truncated pyramids but also for open geometries like in hole flanging. This leads to a pile-up of material and, respectively, an increase in thickness in the undeformed sheet metal [21–24].

To gain a deeper understanding of the characteristics of the ISF hemming process, a numerical model for forming of stretch and shrink hems is to be developed. The hems were previously investigated for their material flow in terms of elongation and thickness change [20]. Because of this, there are already established findings that can be expanded by profound strain measurements using the visioplastic method. On one hand, these measurements enable direct conclusions about the final strains. On the other hand, the results can be used to validate the numerical model in addition to geometric comparisons. Furthermore, detailed insights into the stress–strain state and material flow can be obtained

through simulations. In a subsequent section of this work, the developed models are used to compare the already-established roller hemming and the novel ISF hemming, which is further validated by the experiments. Experiments and numerical simulations are then used to compare the forming results of both hemming processes on a straight hem and to highlight the respective characteristics.

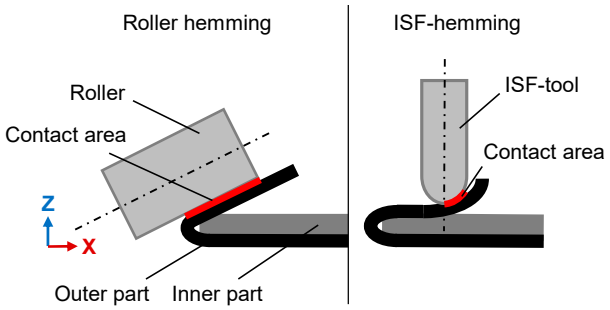

Figure 6. Schematic contact area while hemming for roller hemming (**left**) and ISF hemming (**right**).

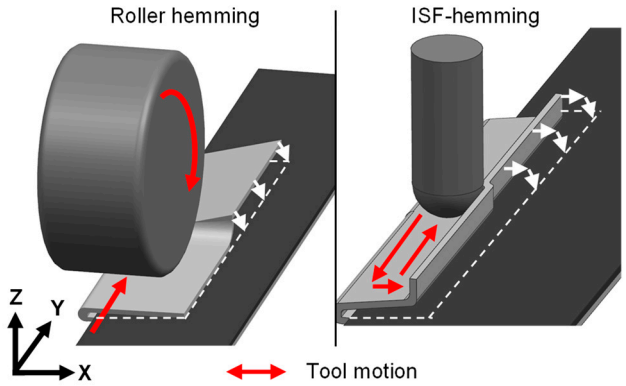

Figure 7. Tool motions of roller hemming (**left**) and ISF hemming (**right**) [20].

2. Materials and Methods

2.1. Material

The material used for the experiments in this work is cold-rolled deep drawing steel DC04 (1.0338) with a thickness of 1 mm, as in the previous work [20]. The grade has excellent deep-drawing properties under all types of deformation and is therefore suitable for high forming requirements. Typical areas of application are internal and external automotive parts formed via bending or deep drawing. DC04 has also proven itself for ISF applications [25,26]. The properties of DC04 are listed in Table 1 and the stress–strain curve is shown in Figure 8.

Table 1. Data sheet for mild steel DC04.

Material: mild steel DC04 (1.0338/St14O3)				
Mechanical Properties				
Density ρ	Yield strength $Rp_{0,2}$		Tensile strength R_m	Elongation A_{80}
7.85 kg/dm^2	140–210 N/mm^2		270–350 N/mm	38%
Chemical Composition (in weight%)				
Element:	C	Mn	P	S
Max:	0.08	0.4	0.03	0.03

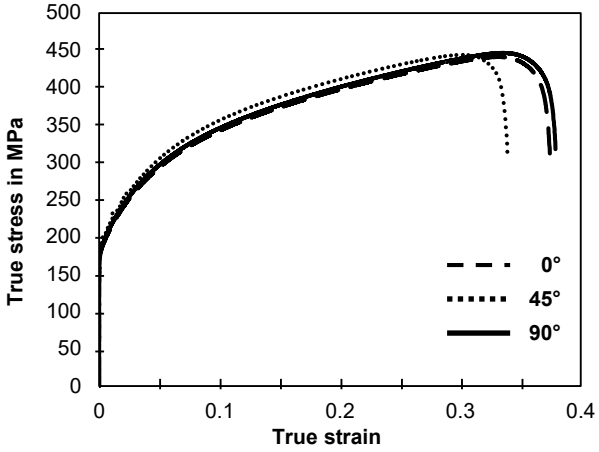

Figure 8. True stress–true strain relation of DC04 sheet [20].

2.2. Tools

The experiments were carried out on an AMINO® DLNC-RB forming machine with exchangeable dies for each hem geometry. For flanging and ISF hemming, a rigid forming tool of 20 mm diameter was used. Because the forming machine only operates on 3 axes and is not able to angle the tools, special tools were designed to implement the roller hemming process. For three-stage hemming, exchangeable rollers with wall angles of 60°, 30°, and 0° were designed and fixed in a universal tool holder. The roller diameter was set to 45 mm at the contact point to the flange, as this showed the best results in previous works [10]. The tools used for all experiments are shown in Figure 9.

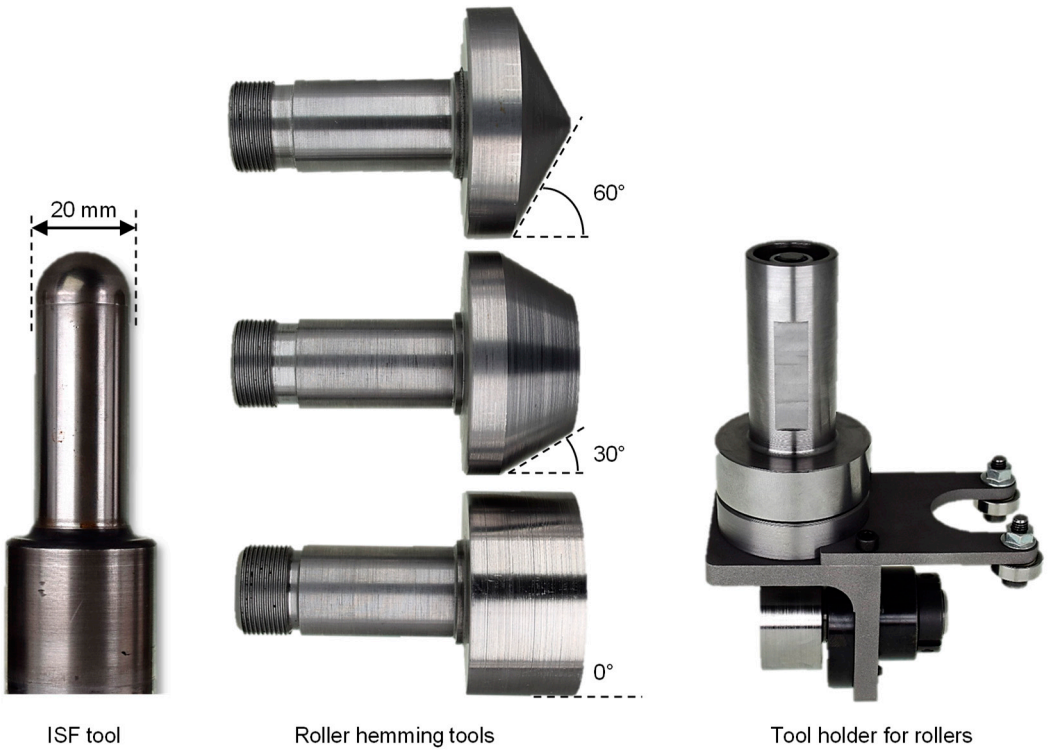

Figure 9. Forming tools.

2.3. Hem Geometries

This work focuses on three hem geometries: straight, (closed) stretch, and (closed) shrink hems. The hem types as well as their corresponding flanges and dies are shown in Figure 10. Moreover, Figure 11 and Table 2 provide an overview of the dimensions of

the specimen used. For the straight hems, a flange length of 20 mm and a flange width of 60 mm was selected. The stretch and shrink hems were set to an initial radius of 50 mm and flange length of 10 mm, as this has shown good results in previous works [20]. All parts were fabricated using cold forming oil Multidraw 472 as lubricant to reduce friction to a minimum.

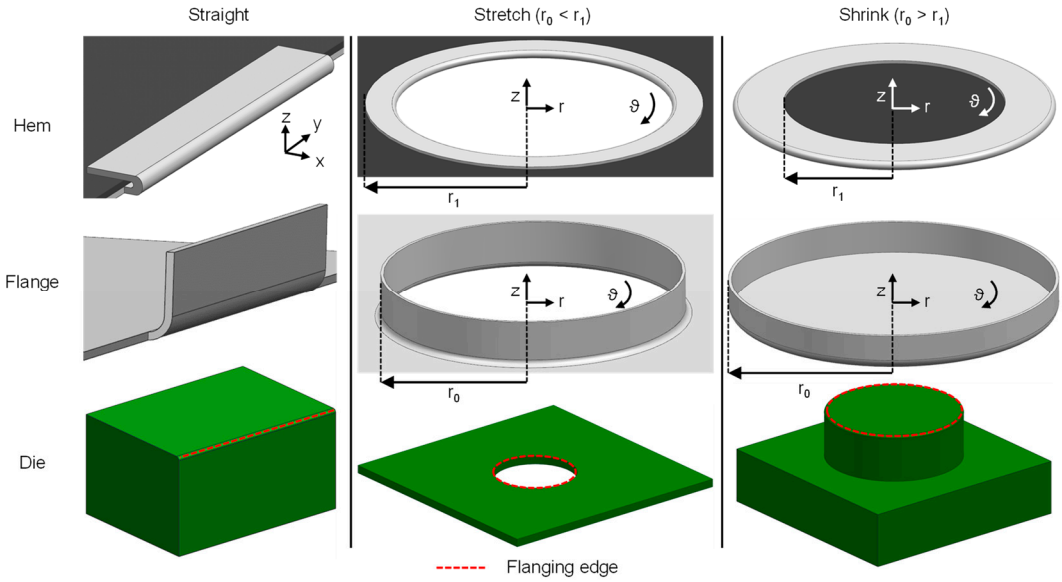

Figure 10. Hem geometries in this work.

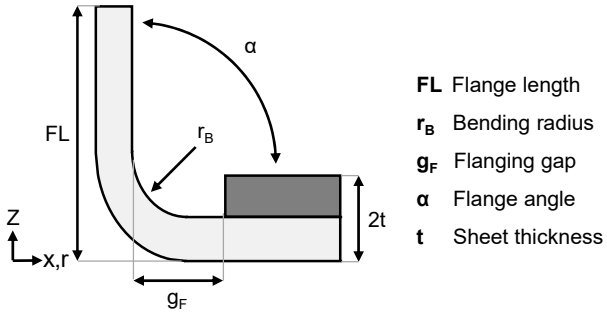

Figure 11. Geometric definitions of the flanges [20].

Table 2. Design of specimen.

Geometry	r_B (mm)	g_F (mm)	α (°)	t (mm)	r_0 (mm)	FL (mm)
Straight	2	2	90	1	-	35
Stretch					50	10
Shrink						

2.4. Experimental Setup and Tool Paths

For the later hemming, the specimens must first be flanged. The flanging was also carried out with ISF. Therefore, the precut sheet metal blanks were fixed between a die and a blank holder, as shown in Figure 12. The flange was formed by the continuous motion of the CN controlled forming tool along the part contour with an increasing depth. The incremental forming parameters were chosen based on the literature and showed good results in previous work: single-stage forming with a tool diameter of 20 mm and a vertical step size (z_V) of 1 mm was set as the tool path strategy for flanging [19,27]. Exemplary tool paths are shown in Figure 13.

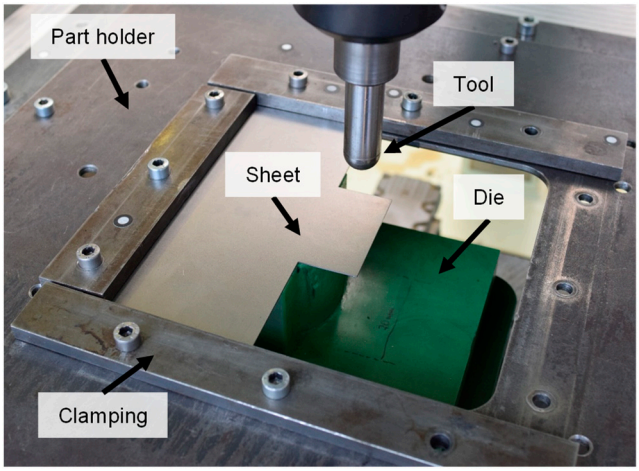

Figure 12. Experimental setup as an example of straight geometry.

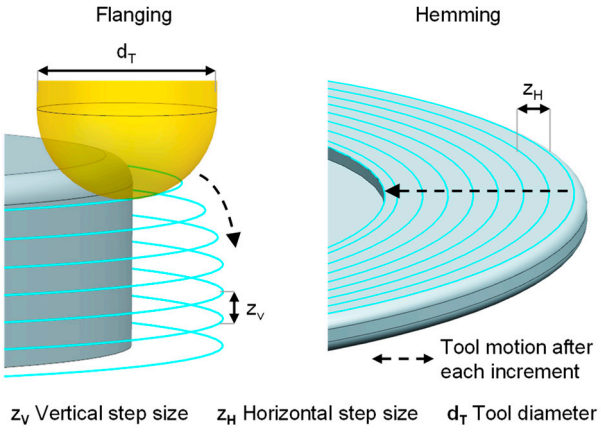

Figure 13. Exemplary tool paths for ISF flanging and hemming [20].

After flanging, the specimens were flipped, and an inner sheet was inserted. Then, hemming was resumed, as shown in Figure 14. The dimensions of the inner sheet were chosen so that a gap (g_F) of 2 mm to the flange remained. ISF hemming was realized by successive horizontal lanes with a horizontal step size (z_H) of 1 mm and no vertical offset (cf. Figure 13).

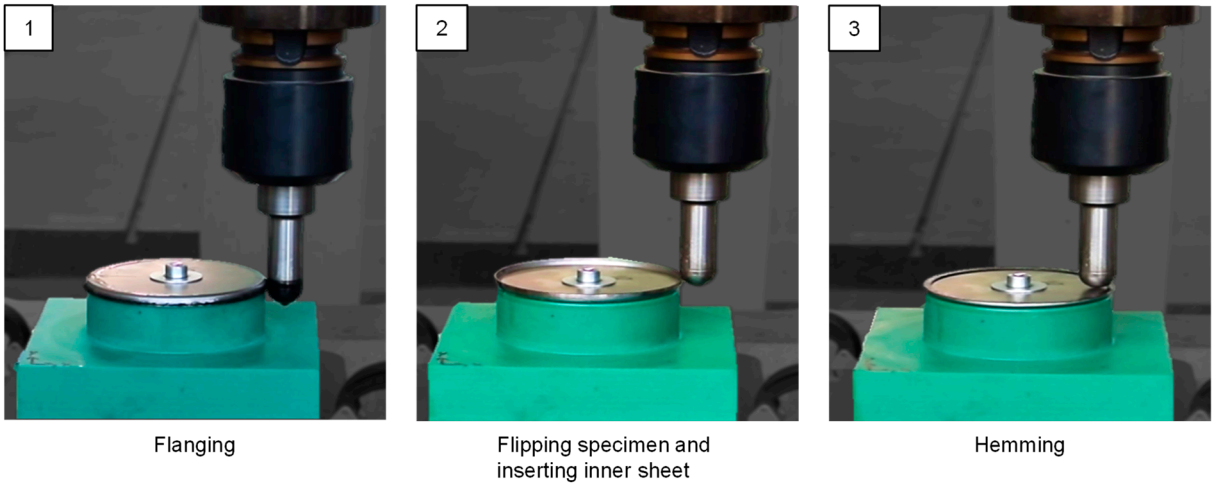

Figure 14. Procedure for ISF hemming as an example of shrink hem geometry [20].

For roller hemming, the upright flange is formed over in multiple stages by rollers with different angled walls, as shown in Figure 15. The rollers drive in a straight path along the sheet edge. The roller in the first and second pre-hemming steps move in the same direction, while the final hemming occurs in the opposite direction. This is implemented to prevent warping of the hem edge.

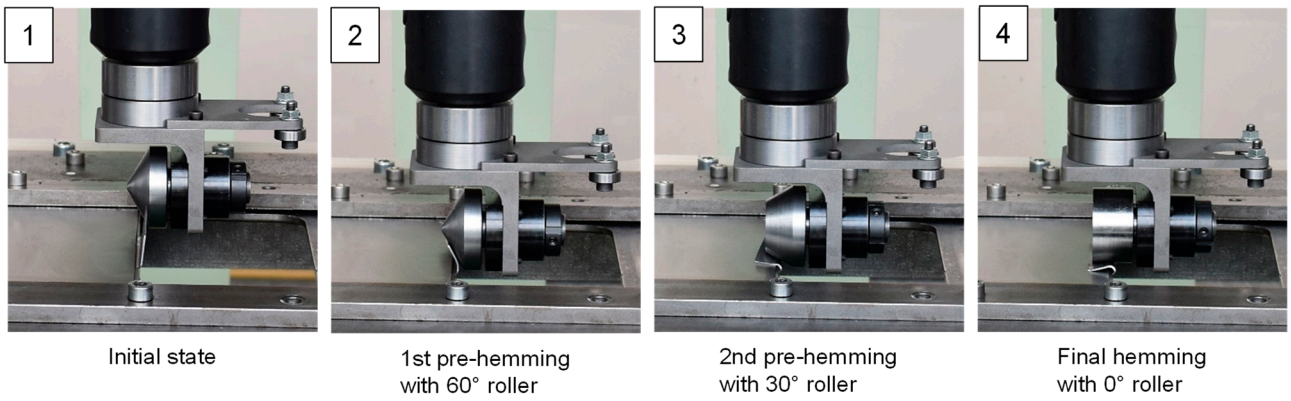

Figure 15. Procedure for roller hemming of the straight hem.

2.5. 3D Scanning

To evaluate the shape of the produced specimens and carry out comparisons to numerical simulations, the specimens were scanned with the Creaform HandyScan 700 from AMETEK GmbH (Leinfelden-Echterdingen, Germany) [28]. The scanner captures and digitalizes 3D shapes with its combined camera and laser system. In this work, the outer geometry as well as the cross-sections of the hems were scanned to allow for geometric comparison to the simulation results. Figure 16 shows the usage of the 3D scanner.

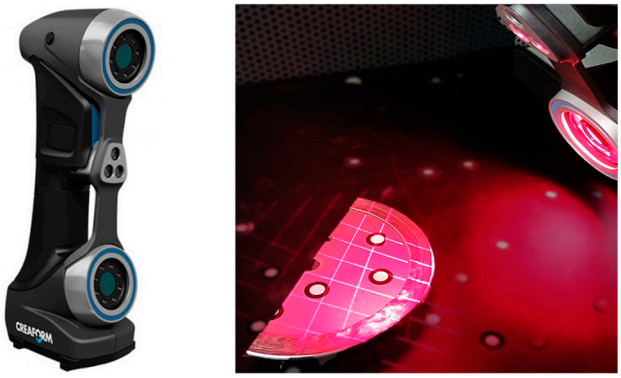

Figure 16. Creaform HandyScan 700 (**left**) and exemplary 3D scanning setup up (**right**) [28].

2.6. Optical Forming Analysis

Part of the evaluation of the hems is the optical deformation measurement. It allows for quantifying the deformation and gaining insight into the strain state. Therefore, a dot pattern (1 mm point diameter with 2 mm point distance), as seen in Figure 17, was applied on the inside of the specimens by a marking laser. After forming, the hems were cut open to reveal the pattern and to photograph it. The distortion of the pattern was then measured, and strains were calculated with the Zeiss Argus system [29].

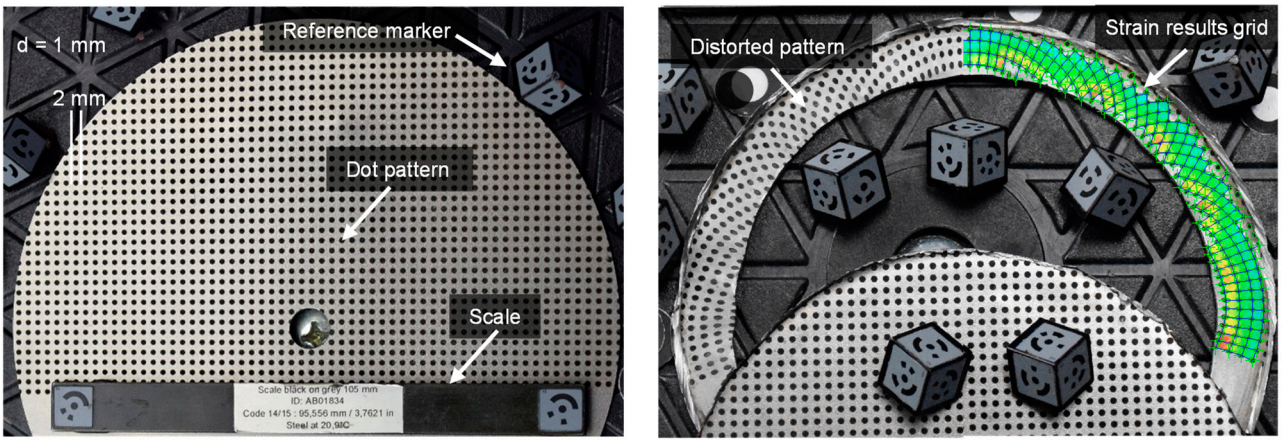

Figure 17. Exemplary optical forming analysis for the shrink hem.

Strain measurement posed certain challenges. Since the method requires a pattern to be applied to the sheet, care must be taken to prevent its destruction during the forming process. Considering the tool contact on the surface of the specimens, the pattern must be applied on the inside (non-tool contact side). However, as the inside of the sheet is covered during hemming, the specimen has to be cut open along the hemming radius afterwards to obtain a direct view of the pattern. Thus, some of the measurement points may get lost while cutting or stay hidden under the cutting edge. This might result in incomplete measurements in the area of the hemming radius. On the opposite side, there are gaps in the measurement towards the hemming edge, as some of the measurement ellipses are not fully visible on the sheet edge (cf. Figure 17). In general, only a limited area and limited number of measurement points are available to analyze the hem due to its relatively short length and the need for the pattern to have specific point diameters and distances.

2.7. Finite Element Analysis (FEA)

The experiments conducted in this work were also simulated using finite element analysis. Simulations were performed with the commercial finite element software Ansys LS-DYNA (V2022R1). An explicit model composed of rigid parts for the tools, dies, and inner sheet as well as a deformable blank for the sheet was set up as presented in Figure 18. The sheets were modeled using shell elements with 1 mm thickness, 0.5 mm element length, and five through-thickness integration points (NIPs). NIPs were selected according to previous studies reported in the literature [30,31]. The element formulation was set to Belytschko–Tsay with thickness stretch (ELFORM = 25) to take the changes in thickness during forming into account. All contacts were defined as AUTOMATIC_SURFACE_TO_SURFACE. The blank holder was considered by fixed nodes around the blank to serve as the clamping. For the material properties, the MAT024-PIECEWISE_LINEAR_PLASTICITY backed with a defining flow curve of DC04 steel was implemented. As the simulations aimed to recreate the actual experiments, the flanging process was also modeled, and its results as stress, strain, and thickness distribution were imported to the initiation of the hemming simulations. Figure 19 shows the results for the stretch and shrink geometry after flanging, which were then used in the hemming simulation. Springback effects were taken into account for both the flanges and the hems by allowing for free recovery in the forming area without constraining nodes.

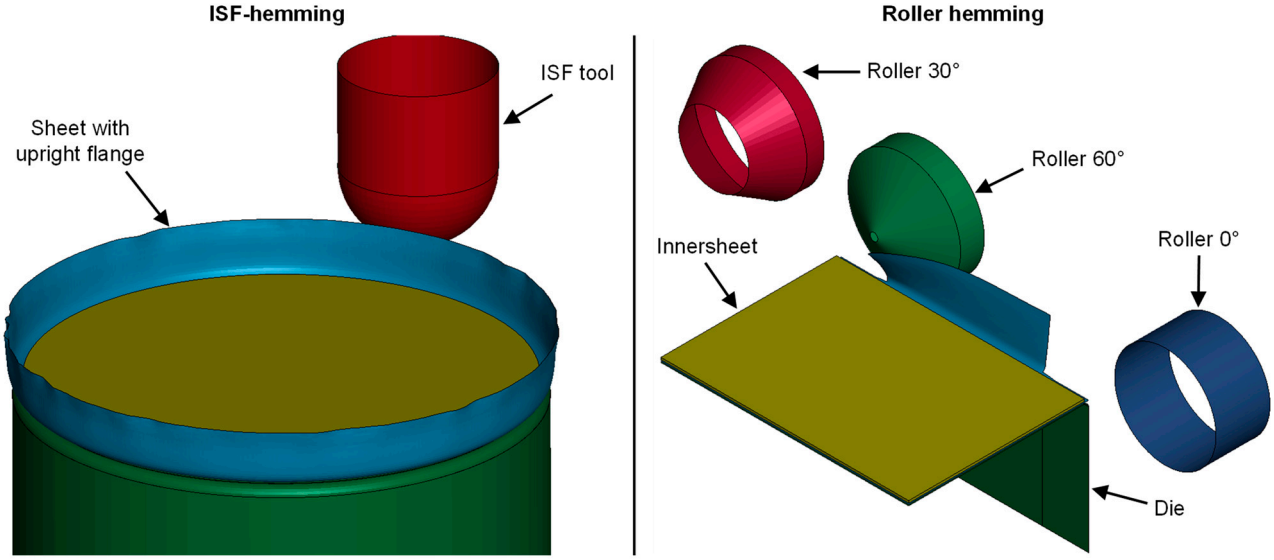

Figure 18. Exemplary setup for ISF hemming (**left**) and roller hemming model (**right**).

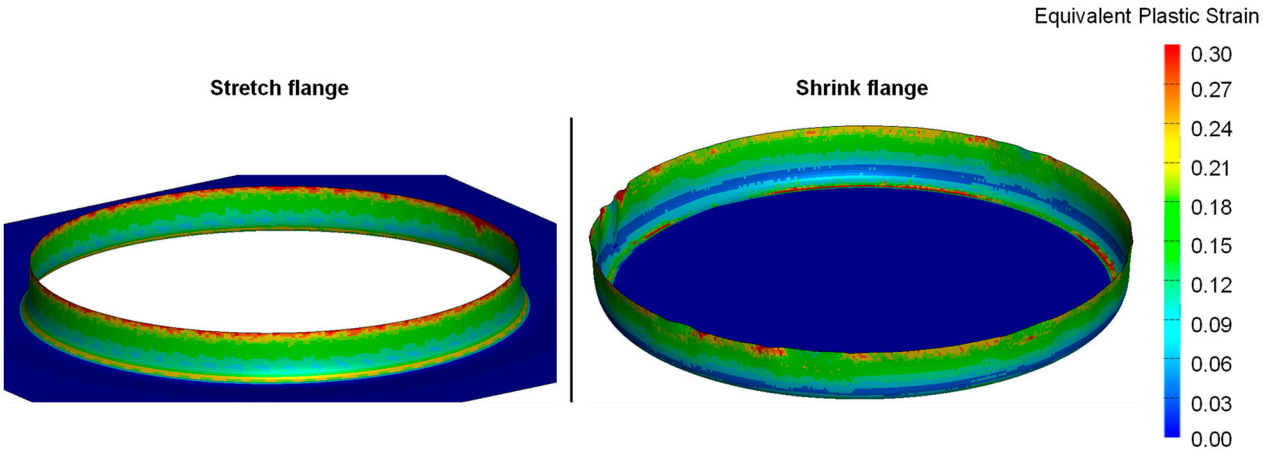

Figure 19. Equivalent plastic strain in stretch (**left**) and shrink (**right**) specimen after flanging simulation.

3. Results

3.1. Validation of ISF Hemming of Curved Hems

In order to validate the model, the simulation results were first compared with experimental measurements in terms of geometry, thickness distribution, and strains. Figure 20 shows the geometric comparison of the cross-sections for the stretch and shrink hem. The shell mid-plane was exported from the simulation results and aligned with the contour of the actual hems captured from a 3D scan via a best-fit method. The flat and undeformed regions were used as a reference for the best fit. This allows for better valuation of the hem contour and hem radius, though it neglects the roll-in/roll-out of the part. In general, the cross-sections show very good agreement, as the height and length of the hems match very well. The curvature of the hem, as was the case with the stretched hem, was also reproduced correctly. The most apparent deviations were observed in the hem radius. This may be due to simplified assumptions made during the simulation of the inner sheet, which was defined as rigid to reduce the calculation effort and time. Consequently, the lower section of the hems appeared to be flat. As shown in the cross-sections of the experimental hems, it cannot be entirely ruled out that the inner sheet was slightly deformed, allowing for the hemming radius to lift slightly.

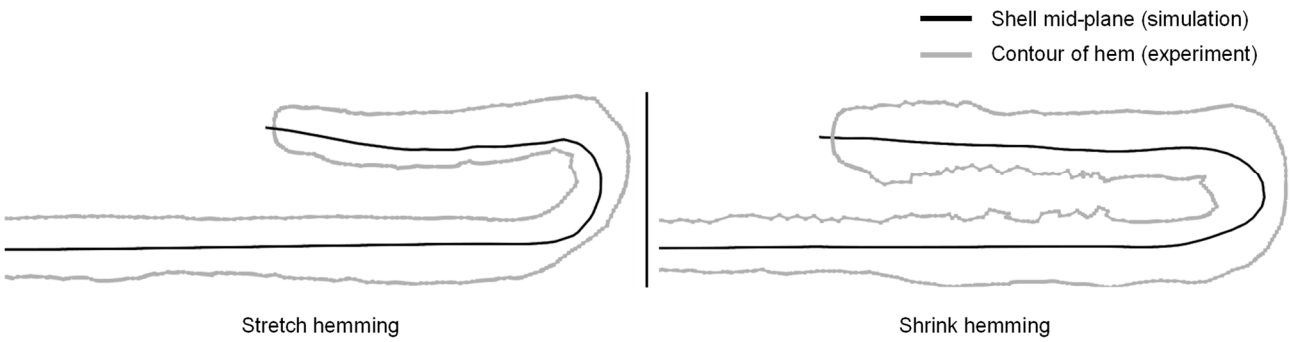

Figure 20. Geometric comparison of experiment and simulation based on the hem cross-sections.

In addition to geometry, the sheet thickness distributions were also analyzed. Building on the results of previous work, the sheet thickness from the simulation results was evaluated and compared to the experimental data [20]. To achieve this, the thickness of the hems was initially measured from the outermost point of the hem edge to the hemming radius. The sheet thickness was then plotted over the measured length for both the experimental and the simulation data, as shown in Figure 21.

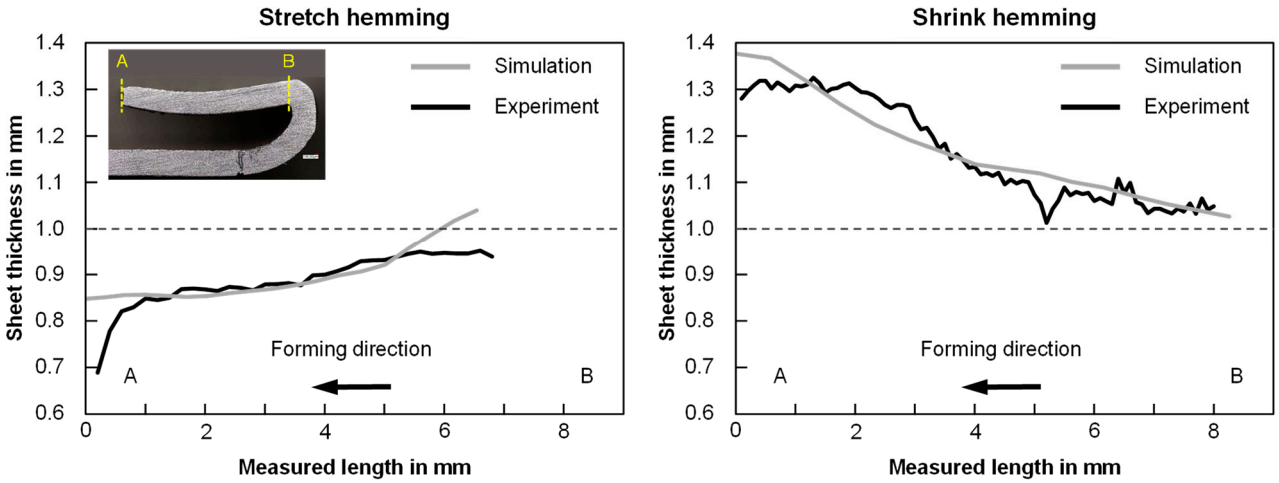

Figure 21. Sheet thickness distribution from experiment and simulation for stretch (**left**) and shrink hems (**right**). The initial blank thickness of 1 mm is indicated by the dotted line.

Previously, it was shown that stretch hemming results in a significant thinning and shrink hemming leads to increased thickness [20]. This behavior was also reproduced to a considerable extent by the simulation, where good agreement with the experiment was found in the middle section of the hems. Greater deviations were present at the hem edge and towards the hem radius. This may be due to the actual shape of the hem. As Figure 22 implies, there was a material drag in one-third of the sheet thickness from the point of tool contact. This may be due to shear in the tool contact surface, but it definitely changes the shape of the hem and influences the thickness measurements. At this point, the simulation model is unable to replicate this characteristic, where the shell elements only simulate the neutral fiber and cannot display surface effects such as this material drag.

For further validation, strain measurements were conducted and compared to the simulation. As described before, the specimens were cut open and the distorted pattern was analyzed by optical deformation measurement. Subsequently, the effective strains could be determined and used as reference values for the simulation. This was also carried out for the stretch and shrink hems, and the results are shown in Figures 23 and 24.

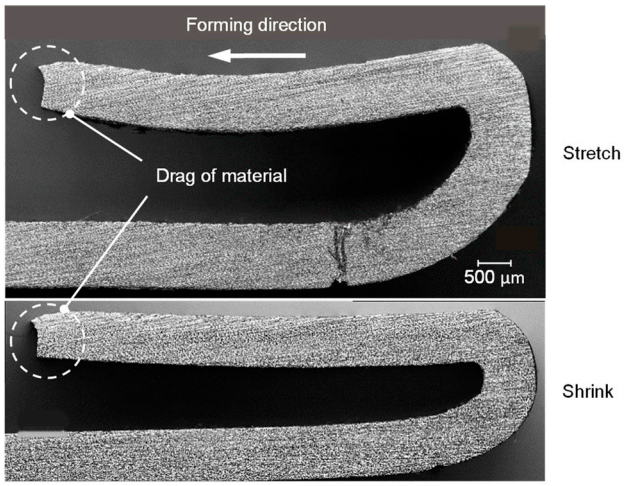

Figure 22. Material drag at the outer edge of hems [20].

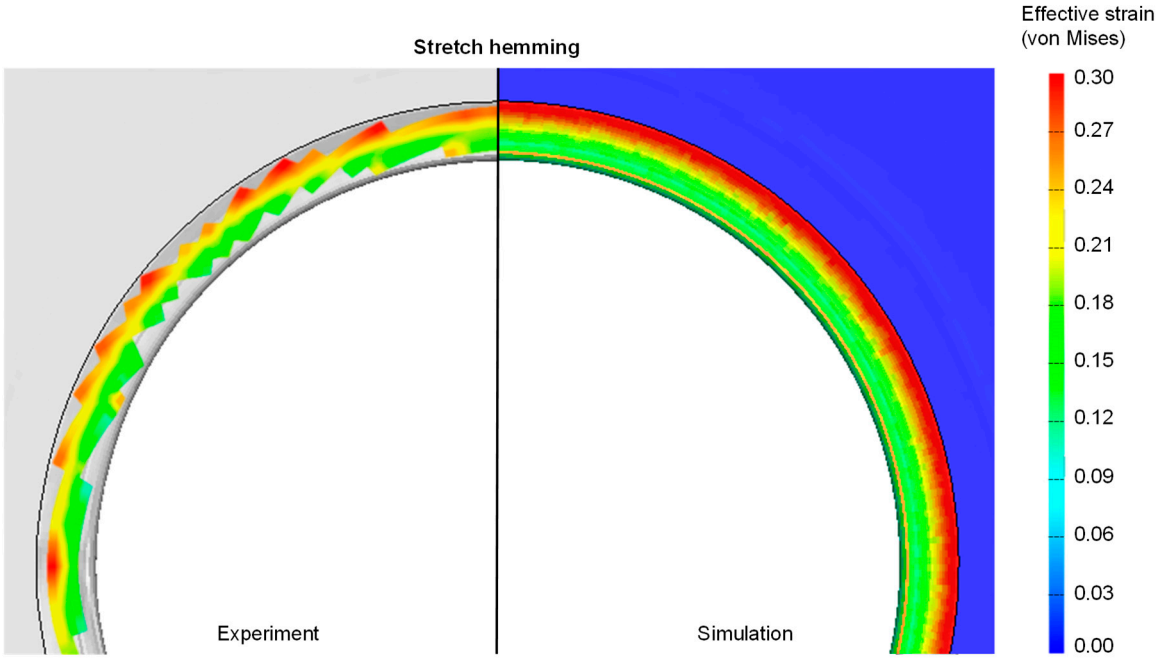

Figure 23. Comparison of effective strains from experiment and simulation for stretch hem.

The simulation accurately predicted the strain distribution for both hem geometries, although the measurement had blind spots, as described in the optical forming analysis chapter. For stretch hemming, the increasing effective strain from hem radius to hem edge, reaching a maximum of approximately 0.3, was in good agreement with the measurements from visioplastic analysis. Additionally, the strain distribution appeared homogeneous in the circumferential direction in both cases.

In the case of the shrink hem (Figure 24), the simulation reflects the trend accurately as well. The lowest strains in the hem radius as well as the peaks in the hem edge were apparent in both analyses. The maxima of approximately 0.5 was found in the areas with the highest compression. In this case, the effective strains were not distributed homogeneously in the circumferential direction.

Apart from the mentioned limitations, the results look very promising, as the geometry, thickness distribution, and strain measurements show the same properties and tendencies as the hems in the experiments and simulation. The results imply that the finite element simulations represent the experiments close enough to be used for further investigation.

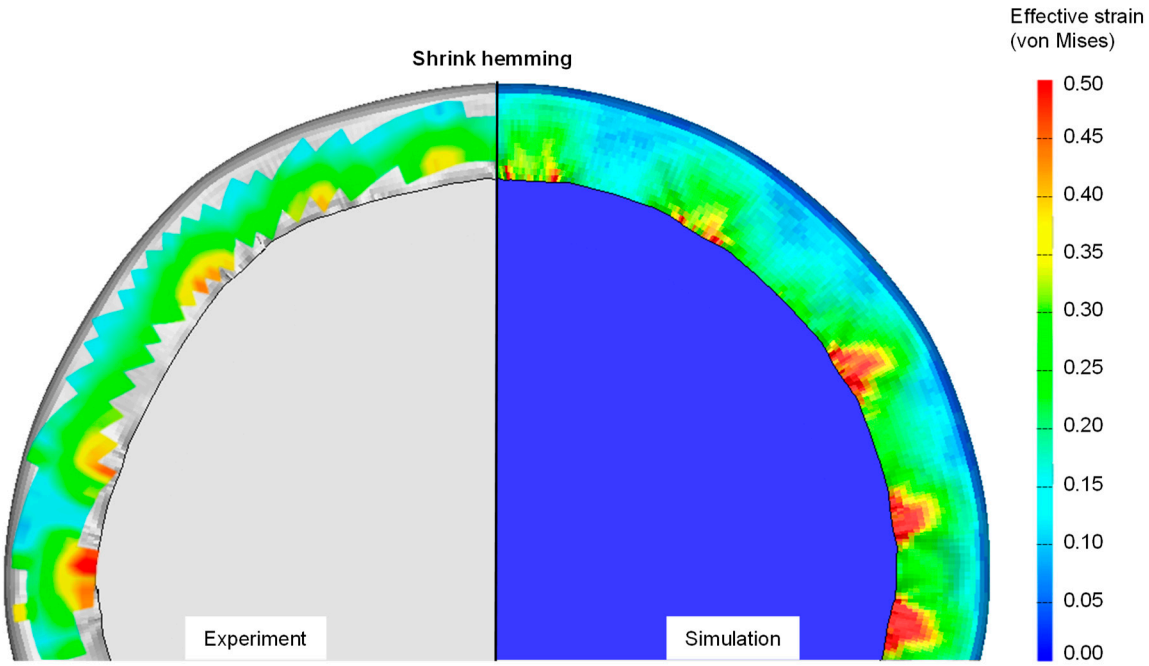

Figure 24. Comparison of effective strains from experiment and simulation for shrink hem.

3.2. Material Flow in ISF Hemming of Curved Hems

Due to the good agreement between the experiments and the model, further analyses can be taken into account. In this way, the simulation provides a deeper insight into the results of incrementally formed hems, which would be difficult to obtain through experiments alone. For example, by considering the vectors of principal strain, conclusions can be drawn about the material flow in the hem. This is illustrated for the stretch hem in Figures 25 and 26. As the major in-plane strains show, the largest deformation is in the tangential direction, reaching up to 0.40. This is expected in stretch forming, as the radius of the hem edge increases. Additionally, the minor principal in-plane strains indicate compression of up to 0.20 in radial direction. The distribution of the strains is also homogeneous in circumferential direction, as previously demonstrated by the effective strains in Figure 23. On the left side, a certain asymmetry of the results is evident. This is due to the point at which the tool changes direction to circle the flange.

The deformation vectors show that the tensile strains are predominant in tangential direction and compression in radial direction. This result is not clearly consistent with the observations from the previous work, as the compression here indicates a reduced flange length after hemming, whereas a slight elongation of the hem was measured previously [20]. The explanation for this can be found in the measurement method in the experiment, where the flange length was measured along the outer edge of the hem. The simulation, on the other hand, only considers the neutral fiber for the mid-plane of the shell element. This results in a difference in the measured length. Further, as already mentioned, there is a surface effect of the dragged material, which was taken into account in the length measurement of the experiment but not in the simulation.

Contrary to this, the strains of the shrink hem in Figures 27 and 28 show compression in the circumferential direction. Similar to the effective strains, the distribution of the in-plane strains is inhomogeneous. At up to 0.60, the strains achieved are significantly greater than with stretch hemming. Furthermore, it becomes apparent that there are tensile strains in radial direction. Those reach up to 0.33 in the areas where wrinkles tend to be formed. Although there are greater compressive strains in the tangential direction in the areas that tend to form wrinkles, the material flow in the forming direction is still recognizable. This is shown on one hand by an increase in flange length and is also supported by the deformation vectors from the simulation.

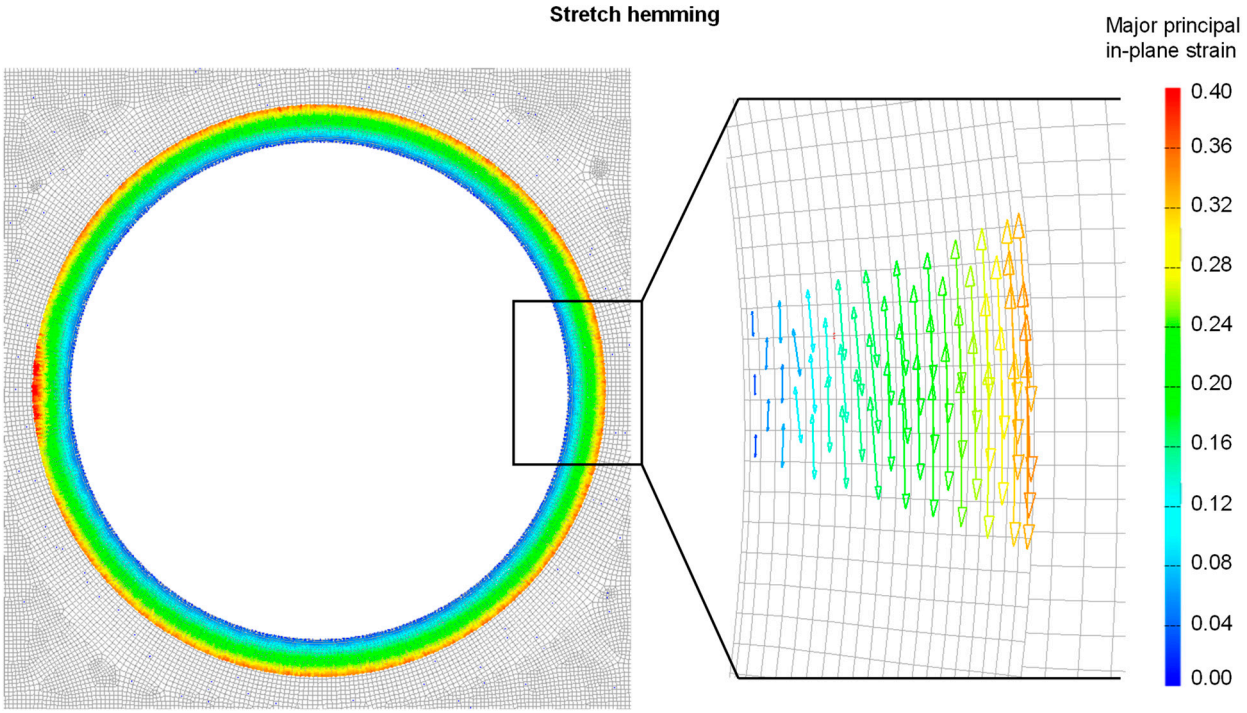

Figure 25. Vectors of major in-plane principal strain for stretch hem.

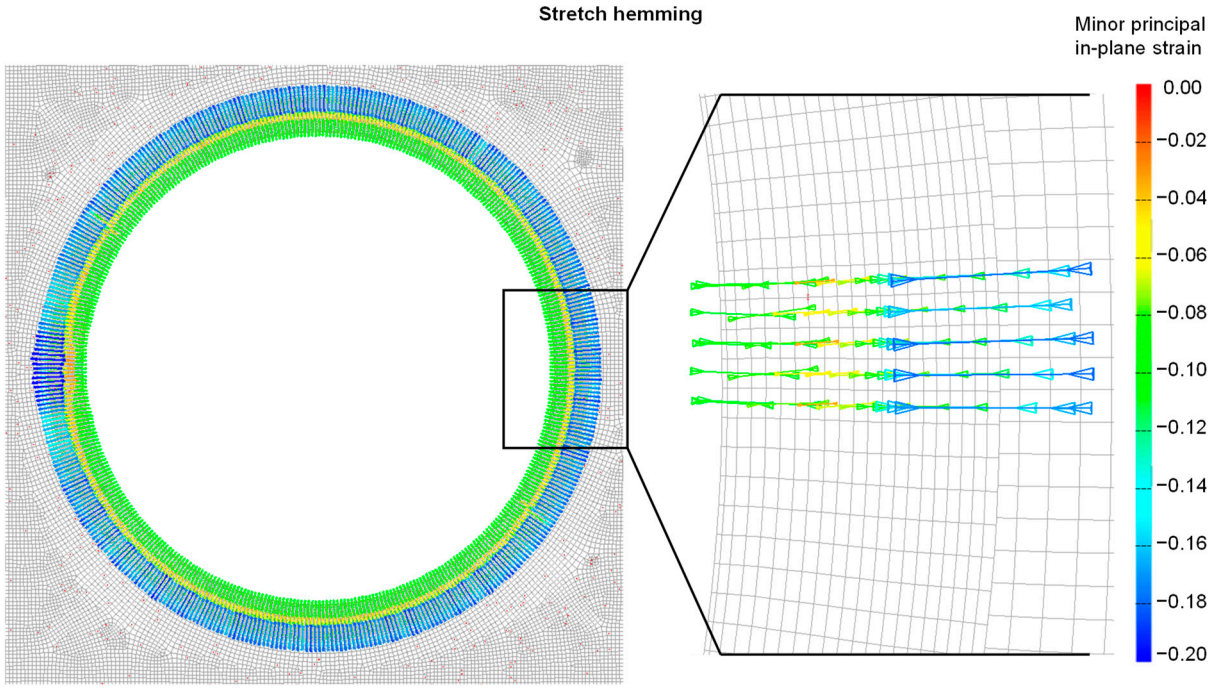

Figure 26. Vectors of minor in-plane principal strain for stretch hem.

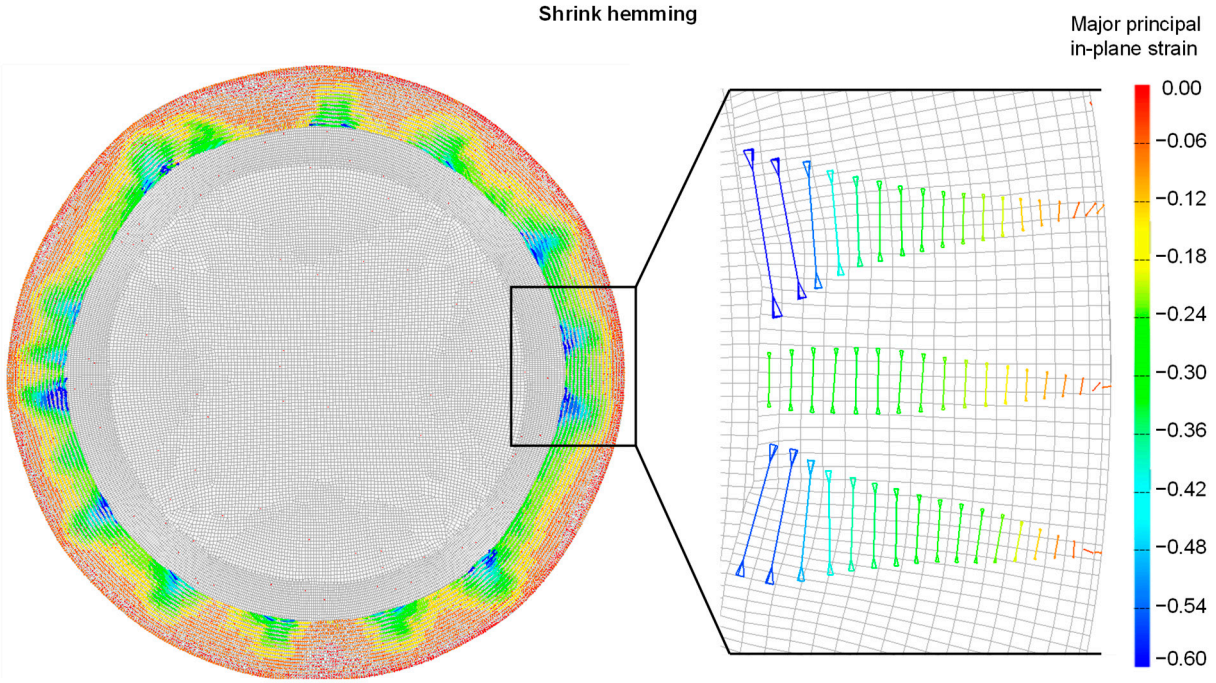

Figure 27. Vectors of major in-plane principal strain for shrink hem.

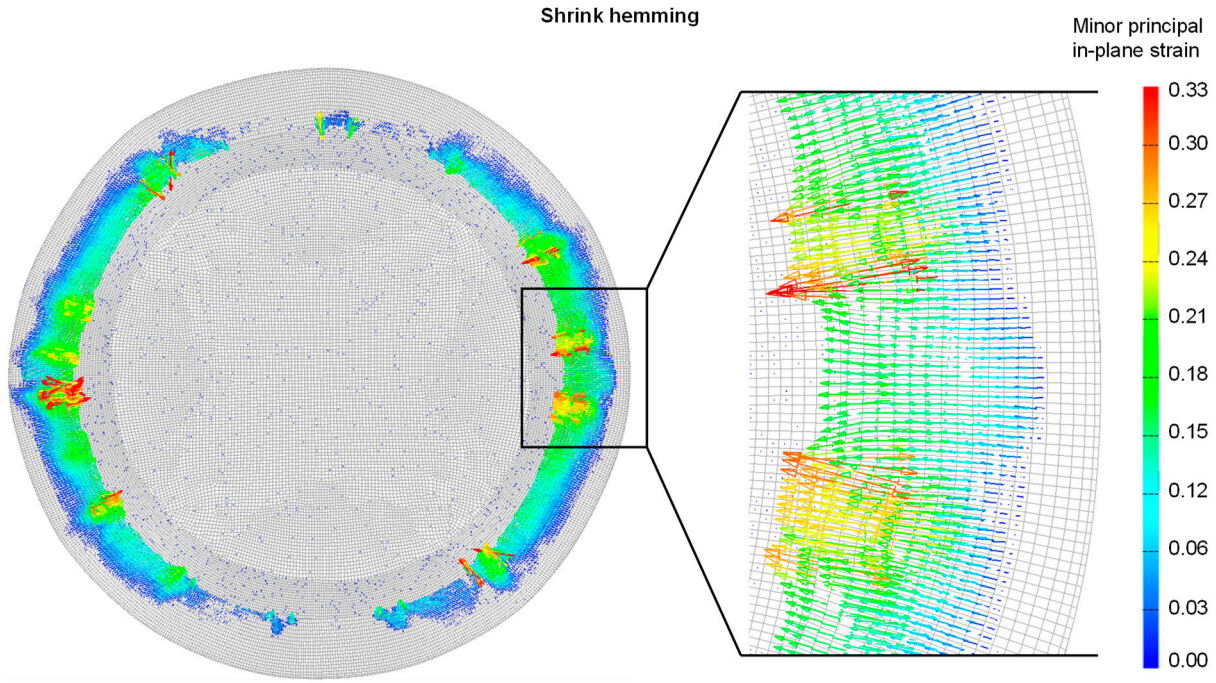

Figure 28. Vectors of minor in-plane principal strain for shrink hem.

Consideration of the strains in the thickness direction provides further evidence to the apparent material flow. As seen in Figure 29, the vectors of deformation show a compression for the stretched hem (thinning) and tension for the shrink hem (thickening). Both characteristics increase towards the hem edge and are consistent with the thickness distributions (cf. Figure 21). Once again, the strains for shrink hemming are significantly greater than for the stretched hem

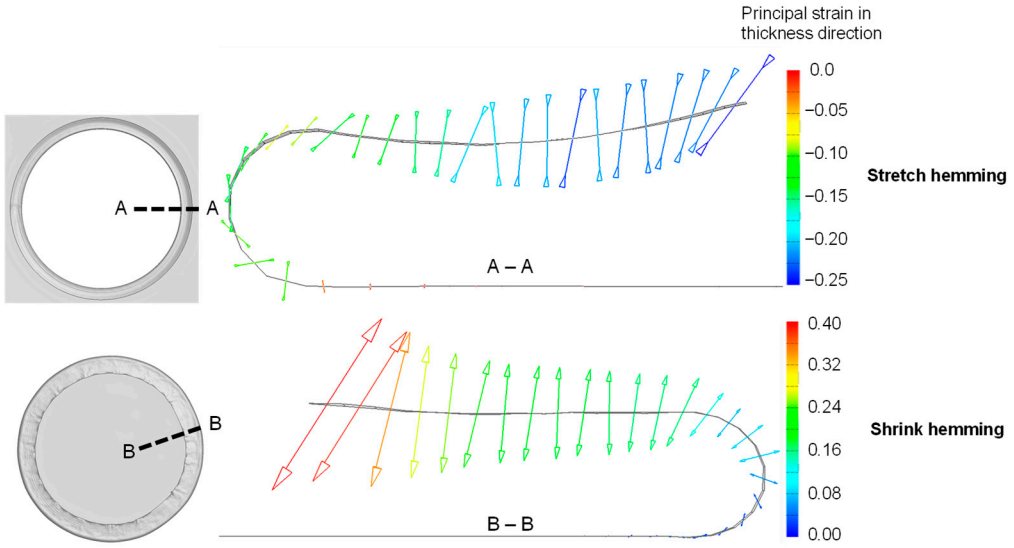

Figure 29. Vectors of strains in thickness direction for stretch and shrink hemming (bulge).

Taking into account all observations regarding the strains in the ISF hemming of curved hems, Figure 30 attempts to summarize the resulting material flow on a generic volume element. As both hem types indicate, the greatest strains are in the tangential direction due to the change in diameter. The change in the thickness direction is significant, and strains in the radial direction are also detectable. ISF hemming facilitates the distribution of tangential strains to compensate for the surface enlargement, therefore preventing cracks in stretch hemming and at the same time offering the degree of freedom that allows for the material to flow out of the thickness, as the vectors of the second principal strain indicate. The same counts for the shrink hem. Global and local elongation of the hem can be seen, and the excess material flows in thickness direction. Joining by ISF made it possible to distribute the material advantageously and at the same time allow for the hem to be thickened to avoid wrinkles.

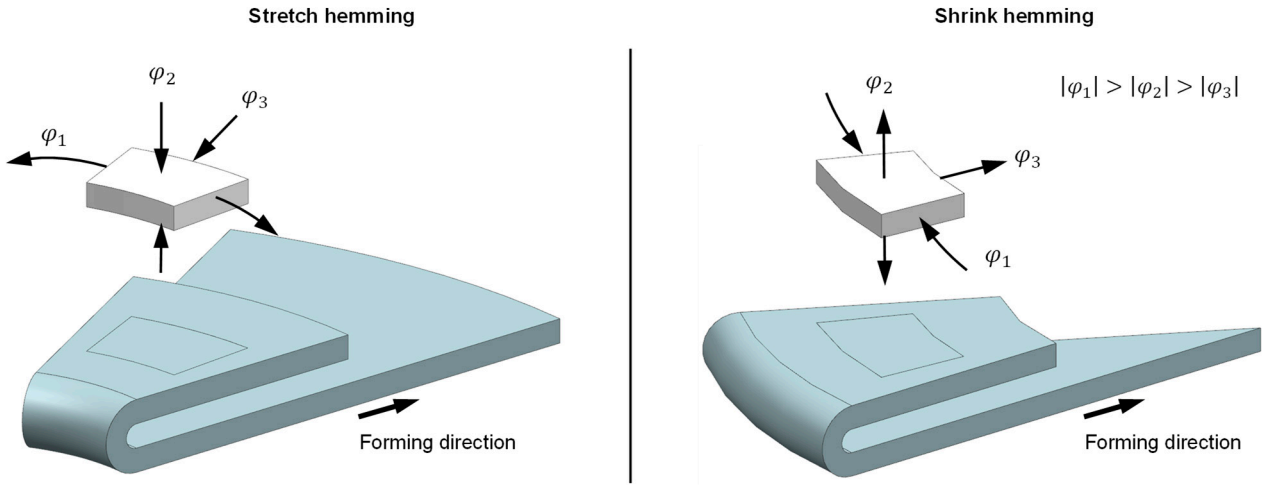

Figure 30. Schematic of resulting material flow vectors in ISF hemming for stretch and shrink hems.

3.3. Comparison of ISF Hemming and Roller Hemming

In order to compare the novel ISF-hemming with conventional roller hemming, experiments were conducted on straight hemming edges with a flange length of 35 mm. This geometry allows for better comparability, as there are fewer geometric constraints than in curved hems. Thereby, process management is also simplified, because the tools only have to follow straight lines in order to bend the flanges. Figure 31 shows the produced

specimens for ISF hemming and roller hemming. In the case of ISF hemming, the surface showed characteristic grooves from the forming process, whereas the roller tool left a single distinct imprint on the hem, as it did not cover the hole flange while forming. Moreover, a slight wave shape could be seen in the roller hemmed specimen, while the ISF-hemmed specimen appeared to be rather flat with a light lift on the lateral edges. Despite the rather long flange length of 35 mm, the ISF-hemmed specimen shows better flatness.

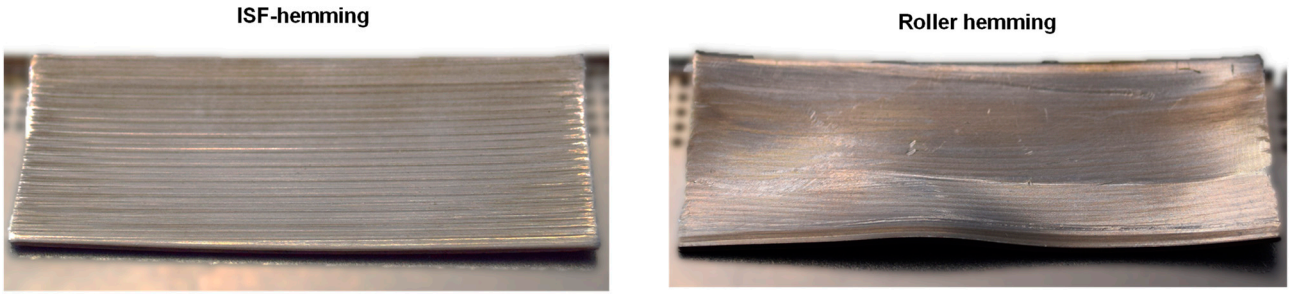

Figure 31. General appearance of the straight hems produced with ISF hemming (**left**) and roller hemming (**right**).

Similar to the closed curved geometries, optical strain measurements were carried out as described in Materials and Methods, and the results are shown in Figure 32 to compare both processes. The measured strains reach up to 8% for the straight geometry, which is significantly lower than for the curved hems. Moreover, the strain maxima are located near the hemming radius for both processes, as is to be expected. In contrast to pure bending, strains are also present in the hem area. In case of ISF hemming, the strain distributes evenly in a convex shape and decreases from approximately 6.5% to 0.5% in the direction of the hem edge. In roller hemming, the strain localizes where the roller indents the flange. In general, the strain values reach up to approximately 4% in the roller-hemmed specimen.

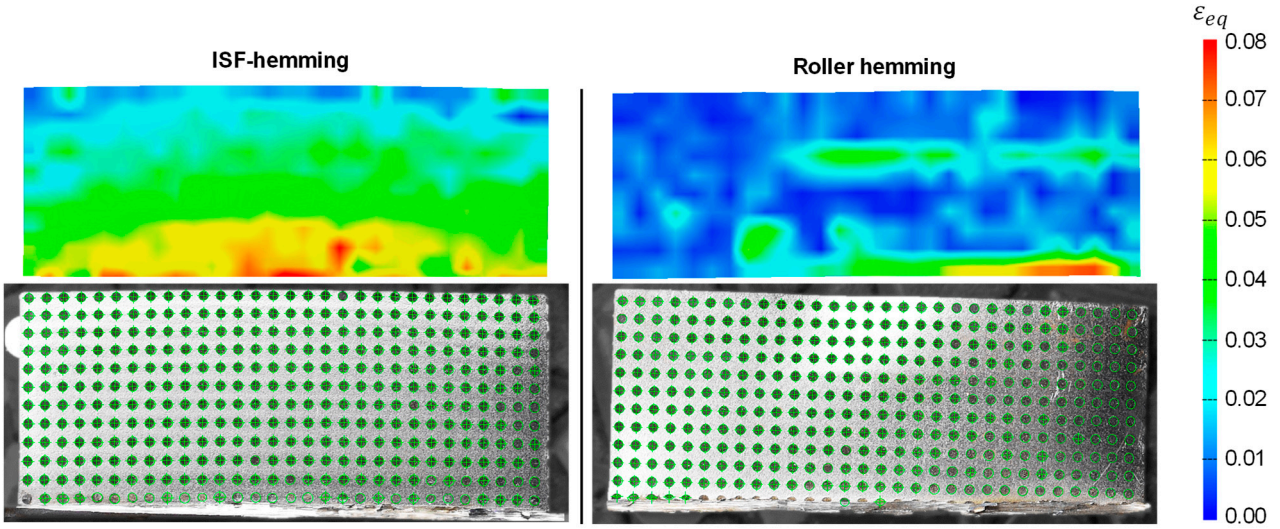

Figure 32. Optical strain measurement for straight hems formed with ISF hemming (**left**) and roller hemming (**right**).

The described observations indicate that there is increased forming in the hem area in ISF hemming. As the entire flange is formed over by the ISF tool, generally, greater strains are detected over the whole hem compared to roller hemming. On one hand, this indicates a different deformation mechanism and material flow, whereas reaching higher strains without failure, and also being able to distribute them, might be beneficial for complex hems, small radii, and corners.

Again, numerical simulations were also set up for ISF hemming and roller hemming of straight hems. In order to gain insights into the deformation mechanism, the analysis focuses on the comparison of the deformation zones in both processes. As shown in Figure 33, the deformation zone is made visible by fringe plots of the so-called pressure in LS-PrePost. In ISF hemming, the deformation zone is divided in half in the forming direction. The half towards the hemming radius, i.e., the part of the hem, which has already been formed, experiences tensile load. The half towards the hem edge, the undeformed region, faces compressive load. This could explain the observations of the change in thickness of the hem, as the material is pushed and pulled away from the hemming radius. This also provides an explanation for the already-discussed drag of material in the outer fiber of the hem.

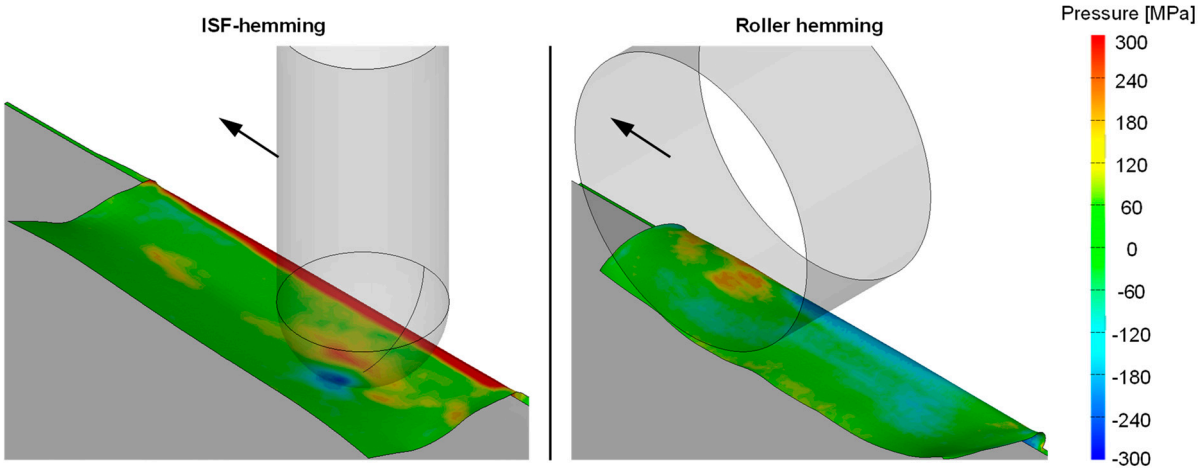

Figure 33. Comparison of the deformation zone in ISF hemming and roller hemming.

In roller hemming, the roller leaves a track of compression as it stretches the material, which slips beneath it. This corresponds very well with observations from the literature that tangential compressive stresses occur, which favor wrinkling or surface waves. This waved surface was observed in the experiment as well as in the simulation. In general, the hem, and in particular the hemming radius, appeared to be pressed onto the inner sheet, while ISF hemming indicated that the hemming radius was rather drawn over the inner sheet.

4. Conclusions

The aim of this work was to gain an in-depth understanding of ISF hemming, a novel joining technology, and to classify it in relation to conventional roller hemming. A combination of experimental and numerical investigations enabled conclusions about the underlying material flow and deformation mechanism. The most important are the following:

- The numerical models in general show a good agreement with the experiments and are able to predict the geometry, thinning behavior, and strain distribution. This makes it a valuable tool for further investigations. Optimization regarding precision, calculation time, and representation of surface effects remain to be further improved.
- In hemming of curved edge parts, strain distributions and material flow vectors contributed to the finding of beneficial material flow. It was shown that ISF hemming allows for greater material flow in thickness direction (φ_2) to reach higher strains before cracking/wrinkling of the hem. Additionally, it facilitates compensation of critical strains by material flow in radial direction (φ_3).
- Investigation of straight hems and comparison with the roller hemming showed that ISF hemming induces strain across the whole hem area, which also reaches higher values than in roller hemming. Both properties can be advantageous for manufacturing complex hems (e.g., with multiple curvature changes) and small radii,

as well as corners. Also, rather long flange lengths (e.g., 35 mm) can be formed without significant limitations, as demonstrated. Therefore, the field of application in joining by forming can be extended with ISF hemming.

- One reason for the differences in the forming characteristic of ISF hemming compared to roller hemming was found in the deformation zone and thus deformation mechanism. It was pointed out that conventional roller hemming comes close to bending; therefore, the predominant deformation in the shell midplane is compression of the hemming radius. Contrary to this, ISF hemming tends to draw the hem, creating tensile load on the hemming radius.

Further research will focus on forming more challenging hems. As an example, the joining of car body panels with multiple curvature changes and sharp corners can be targeted to further prove the benefits of this novel joining technique. Moreover, the influence of the so-called drag of material in the upper third of the sheet thickness remains to be investigated. Numerical models with multilayered solid elements might be able to replicate such surface effects in ISF hemming and help in understanding the underlying mechanism. In future research, the deformation of the inner sheet for the hemming process should be taken into account, because it affects the shape of the joined sheets in the radius zone.

Author Contributions: Conceptualization, D.S. and D.B.; Formal analysis, D.S.; Funding acquisition, D.B.; Investigation, D.S.; Methodology, D.S. and D.B.; Project administration, D.B.; Resources, D.B.; Supervision, D.B.; Validation, D.S.; Visualization, D.S.; Writing—original draft, D.S.; Writing—review and editing, D.B. All authors have read and agreed to the published version of the manuscript.

Funding: Funded by the Deutsche Forschungsgemeinschaft (DFG, German Research Foundation)—459861167.

Data Availability Statement: The data presented in this study are available upon request from the corresponding author.

Conflicts of Interest: The authors declare no conflicts of interest.

References

1. Böllinghaus, T.; Byrne, G.; Cherpakov, B.; Chlebus, E.; Cross, C.E.; Denkena, B.; Dilthey, U.; Hatsuzawa, T.; Herfurth, K.; Herold, H.; et al. Manufacturing Engineering. In *Springer Handbook of Mechanical Engineering*, 1st ed.; Grote, K.H., Antonsson, E., Eds.; Springer: Berlin/Heidelberg, Germany, 2009; pp. 523–785. [CrossRef]
2. Kästle, C.; Liewald, M.; Roll, K. Springback Simulation of the Process Chain Press Line Forming and Roller Hemming Processes. *KEM* **2013**, *549*, 231–238. [CrossRef]
3. Kim, H.; Chatti, S.; Kardes, N. Processes and Applications. In *Sheet Metal Forming*; Altan, T., Tekkaya, A.E., Eds.; ASM international: Tokyo, Japan, 2012; pp. 19–49. [CrossRef]
4. Wang, S.; Li, J.; Li, M.; Zhu, W. Numerical Simulation Method of Roller Hemming on Variable Curvature Aluminium Alloy Sheet with Adhesive. *AMMCS* **2021**, *20*, 399–406. [CrossRef]
5. Drossel, W.G.; Pfeifer, M.; Findeisen, M.; Rössinger, M.; Eckert, A.; Barth, D. The influence of the robot's stiffness on roller hemming processes. In Proceedings of the ISR/Robotik 2014; 41st International Symposium on Robotics, Munich, Germany, 2–3 June 2014; pp. 531–538.
6. Burchitz, I.; Fritsche, D.; Grundmann, G.; Hillmann, M. Efficient planning and numerical analysis of industrial hemming processes. *AIP Conf. Proc.* **2011**, *1383*, 243–250. [CrossRef]
7. Le Maoût, N.; Manach, P.Y.; Thuillier, S. Influence of prestrain on the numerical simulation of the roller hemming process. *J. Mater. Process. Technol.* **2012**, *212*, 450–457. [CrossRef]
8. Ceretti, E.; Attanasio, A.; Fiorentino, A.; Giardini, C. Sheet Hemming with Rolling Tools: Analysis and Optimization of the Part Quality. *KEM* **2007**, *344*, 357–364. [CrossRef]
9. Livatyali, H.; Laxhuber, T.; Altan, T. Experimental investigation of forming defects in flat surface–convex edge hemming. *J. Mater. Process. Technol.* **2004**, *146*, 20–27. [CrossRef]
10. Gürgen, S. A parametric investigation of roller hemming operation on a curved edge part. *ACME* **2019**, *19*, 11–19. [CrossRef]
11. Zubeil, M.; Roll, K.; Merklein, M. Untersuchung der Gefügeentwicklung beim Rollfalzen. In Proceedings of the 17. Sächsische Fachtagung Umformtechnik SFU, Freiberg, Germany, 24–26 November 2010; pp. 149–161.
12. Abe, Y.; Ijichi, W.; Mori, K.-i.; Nakagawa, K. Hemming with Pre-Bent Inner Sheet for Joining Ultra-High Strength Steel Sheets of Automobile Parts. *J. Manuf. Mater. Process.* **2020**, *4*, 77. [CrossRef]

13. Li, J.; Zhu, W.; Wang, S. Numerical Quantification Model and Experiment of External Force on Roller Hemming of Curved Edge Aluminium Alloy with Adhesive. *Chin. J. Mech. Eng.* **2022**, *35*, 17. [CrossRef]
14. Peter, I.; Fracchia, E.; Canale, I.; Maiorano, R. Incremental Sheet Forming for Prototyping Automotive Modules. *Procedia Manuf.* **2019**, *32*, 50–58. [CrossRef]
15. Kajal, G.; Tyagi, M.R.; Kumar, G. A review on the effect of residual stresses in incremental sheet metal forming used in automotive and medical sectors. *Mater. Today Proc.* **2023**, *78*, 524–534. [CrossRef]
16. Seiter, A.; Pofahl, T.; Trautz, M.; Reitmaier, L.M.; Hirt, G. Design and Analysis of Freeform Shell Structures Composed of Doubly Curved Sheet Metal Panels. In Proceedings of the IASS Annual Symposium 2019—Structural Membranes 2019, Barcelona, Spain, 7–10 October 2019.
17. Seyyedi, S.E.; Gorji, H.; Bakhshi-Jooybari, M.; Mirnia, M.J. Comparison between conventional press-working and incremental forming in hole-flanging of AA6061-T6 sheets using a ductile fracture model. *Int. J. Solids Struct.* **2023**, *270*, 112225. [CrossRef]
18. Hussain, G.; Hassan, M.; Wei, H.; Buhl, J.; Xiao, M.; Iqbal, A.; Qayyum, H.; Riaz, A.A.; Muhammad, R.; Ostrikov, K. Advances on Incremental forming of composite materials. *Alex. Eng. J.* **2023**, *79*, 308–336. [CrossRef]
19. Brecher, C.; Özdemir, D.; Weber, A.R. Integrative production technology—Theory and applications. In *Integrative Production Technology*; Springer: Cham, Switzerland, 2017; pp. 1–17.
20. Steinfels, D.; Reitmaier, L.M.; Bailly, D.B. Preliminary experimental investigation on hemming of curved edge parts by means of incremental sheet forming. *Int. J. Adv. Manuf. Technol.* **2024**, *133*, 4879–4891. [CrossRef]
21. Jackson, K.; Allwood, J. The mechanics of incremental sheet forming. *J. Mater. Process. Technol.* **2009**, *209*, 1158–1174. [CrossRef]
22. Hussain, G.; Valaei, H.; Al-Ghamdi, K.A.; Khan, B. Finite element and experimental analyses of cylindrical hole flanging in incremental forming. *Trans. Nonferrous Met. Soc. China* **2016**, *26*, 2419–2425. [CrossRef]
23. Borrego, M.; Morales-Palma, D.; López-Fernández, J.A.; Martínez-Donaire, A.J.; Centeno, G.; Vallellano, C. Hole-flanging of AA7075-O sheets: Conventional process versus SPIF. *Procedia Manuf.* **2020**, *50*, 236–240. [CrossRef]
24. Mezher, M.T.; Khazaal, S.M.; Namer, N.S.; Shakir, R.A. A comparative analysis study of hole flanging by incremental sheet forming process of AA1060 and DC01 sheet metals. *JESTEC* **2021**, *16*, 4383–4403.
25. Mulay, A.; Ben, B.S.; Ismail, S.; Kocanda, A.; Jasiński, C. Performance evaluation of high-speed incremental sheet forming technology for AA5754 H22 aluminum and DC04 steel sheets. *Archiv. Civ. Mech. Eng* **2018**, *18*, 1275–1287. [CrossRef]
26. Mezher, M.T.; Barrak, O.S.; Nama, S.A.; Shakir, R.A. Predication of Forming Limit Diagram and Spring-back during SPIF process of AA1050 and DC04 Sheet Metals. *JMERD* **2021**, *44*, 337–345.
27. Voswinckel, H.; Bambach, M.; Hirt, G. Process Limits of Stretch and Shrink Flanging by Incremental Sheet Metal Forming. *KEM* **2013**, *549*, 45–52. [CrossRef]
28. Creaform HAndyScan700. Available online: https://www.creaform3d.com/en/customer-support/legacy-products/first-generation-handyscan-3d-zscanner-700 (accessed on 21 November 2024).
29. ARGUS Optical Solution for Forming Analysis. Available online: https://www.zeiss.com/metrology/us/systems/optical-3d/3d-testing/argus.html (accessed on 21 November 2024).
30. Le Maoût, N.; Thuillier, S.; Manach, P.Y. Drawing, flanging and hemming of metallic thin sheets: A multi-step process. *Mater. Des.* **2010**, *31*, 2725–2736. [CrossRef]
31. Lenard, J.G. Numerical simulation of sheet metal forming. In *Metal Forming Science and Practice: A State-of-the-Art Volume in Honour of Professor JA schey's 80th Birthday*, 1st ed.; Elsevier Science Ltd.: Oxford, UK, 2002.